PROCEEDINGS OF SCIENCE

# Computing the Adler function from the vacuum polarization function

**Hanno Horch**[*1], **Gregorio Herdoiza**[1], **Benjamin Jäger**[1,2], **Hartmut Wittig**[1,2]

[1] *PRISMA Cluster of Excellence, Institut für Kernphysik, Johannes Gutenberg Universität Mainz, 55099 Mainz, Germany*

[2] *Helmholtz Institute Mainz, Johannes Gutenberg Universität Mainz, 55099 Mainz, Germany*

*E-mail:* horch@kph.uni-mainz.de, herdoiza@kph.uni-mainz.de, jaeger@kph.uni-mainz.de, wittig@kph.uni-mainz.de

**Michele Della Morte**

*CP3-Origins & Danish IAS, University of Southern Denmark*
*Campusvej 55, DK-5230 Odense M, Denmark and IFIC (CSIC)*
*Calle Catedrático José Beltrán, 2. E-46980, Paterna, Spain*
*E-mail:* dellamor@ific.uv.es

**Andreas Jüttner**

*School of Physics and Astronomy*
*University of Southampton, UK*
*E-mail:* a.juttner@soton.ac.uk

We use a lattice determination of the hadronic vacuum polarization tensor to study the associated Ward identities and compute the Adler function. The vacuum polarization tensor is computed from a combination of point-split and local vector currents, using two flavours of O($a$)-improved Wilson fermions. Partially twisted boundary conditions are employed to obtain a fine momentum resolution. The modifications of the Ward identities by lattice artifacts and by the use of twisted boundary conditions are monitored. We determine the Adler function from the derivative of the vacuum polarization function over a large region of momentum transfer $q^2$. As a first account of systematic effects, a continuum limit scaling analysis is performed in the large $q^2$ regime.

CLS based

*31st International Symposium on Lattice Field Theory LATTICE 2013*
*July 29 - August 3, 2013*
*Mainz, Germany*

[*] Speaker.

 

PoS(LATTICE 2013)304

## 1. Introduction

Recently, there has been a lot of interest in lattice determinations of the hadronic vacuum polarization and related quantities, such as the Adler function. The latter can be used to determine the running of $\alpha_{\rm QED}$ [1,2], which is a limiting factor for phenomenological studies at a future linear collider. The Adler function is related to the vacuum polarization function $\Pi(q^2)$ by

$$D(q^2) = -\frac{3\pi q^2}{\alpha}\frac{d}{dq^2}\Delta\alpha^{\rm had}_{\rm QED}(q^2) = 12\pi^2 q^2 \frac{d}{dq^2}\Pi(q^2), \tag{1.1}$$

where $\Delta\alpha^{\rm had}_{\rm QED}(q^2)$ is the shift of the fine structure constant due to hadronic contributions. The vacuum polarization is being extensively studied by means of lattice simulations. The present study reports on a continuation of the project in [3].
In the continuum the Ward identity for the vacuum polarization tensor is given by

$$\sum_\mu q_\mu \Pi_{\mu\nu}(q^2) = \sum_\nu q_\nu \Pi_{\mu\nu}(q^2) = 0. \tag{1.2}$$

On the lattice, these relations are not necessarily satisfied, for instance, due to the use of a local non-conserved current and boundary conditions. In this work we investigate the modifications of the Ward identity due to the use of twisted boundary conditions. The structure of this work is as follows: in section 2 we define the basic quantities used in our study. We discuss the procedures developed to determine the Adler function in section 3. We present our results for the Ward identities in section 4. In section 5 we draw conclusions and give an outlook for the future course of this project.

## 2. The vacuum polarization

In our study we use two dynamical flavours of O($a$) improved Wilson fermions and the Wilson plaquette action. The calculations are performed on gauge configurations generated by the CLS initiative [4]. The ensembles considered in this paper are listed in table 1.

| Label | V | $\beta$ | $a$[fm] | $m_\pi$[MeV] | $m_\pi L$ | $N_{cfg}$ |
|---|---|---|---|---|---|---|
| A5 | $64\times 32^3$ | 5.20 | 0.079 | 312 | 4.0 | 250 |
| E5 | $64\times 32^3$ | 5.30 | 0.063 | 451 | 4.7 | 168 |
| F6 | $96\times 48^3$ | 5.30 | 0.063 | 324 | 5.0 | 217 |
| N6 | $96\times 48^3$ | 5.50 | 0.050 | 340 | 4.0 | 173 |

**Table 1:** List of simulation parameters of the CLS ensembles considered in this work. The configurations were generated with $N_f = 2$, O($a$)-improved Wilson fermions. The lattice spacing is taken from [5].

The hadronic vacuum polarization tensor is defined as

$$\Pi^{N_f}_{\mu\nu}(q^2) = \int d^4x e^{iqx} \left\langle J^{N_f}_\mu(x) J^{N_f}_\nu(0)\right\rangle = \left(g_{\mu\nu}q^2 - q_\mu q_\nu\right)\Pi(q^2), \tag{2.1}$$

with the vector currents $J_\mu^{N_f}(x) = \sum_{f=1}^{N_f} Q_f \bar{\psi}_f(x)\gamma_\mu \psi_f(x)$, where $Q_f$ is the electric charge of each flavour. In the continuum, $\Pi(q^2)$ is related to the vacuum polarization tensor via eq. (2.1), which follows from Euclidean invariance and current conservation. When eq. (2.1) is evaluated on the lattice both connected and disconnected diagrams occur. Despite the fact that the latter are estimated [6,7] to be of the order of $-10\%$, we currently neglect these contributions. Following [3] we impose twisted boundary conditions [8,9,10] on the quark fields

$$\psi(x_i + L) = e^{i\Theta_i}\psi(x_i) \quad \Rightarrow \quad \hat{q}_\mu = \frac{2}{a}\sin\left(\frac{\pi n_\mu}{L_\mu/a} - \frac{\Theta_\mu}{2L_\mu/a}\right), \tag{2.2}$$

where the twist is only introduced in one direction $\Theta = (0,\Theta_1,0,0)$, to tune the momenta. The main benefit of this is the improved constraint on fits in the small momentum region between the first and second Fourier momentum. In the simulations, the twist can be interpreted as a constant background field on the gauge field, $U_\mu^\Theta(x) = U_\mu(x)e^{iaB_\mu}$, where $B_\mu$ is a matrix in flavour space depending on the twist angles. In the case of $N_f = 2$ we have $\psi^T(x) = \left(q^{(1)}, q^{(2)}\right)^T$, thus for our choice of twist angles we find $B_{\mu=0,2,3} = 0$, $B_1 = \mathrm{diag}\left(B_1^{(1)}, B_1^{(2)}\right)$ with $B_1^{(j)} = \Theta_1^{(j)}/L$.
In the lattice regularization there is a certain freedom for the implementation of these currents. We use a combination of local and point-split currents

$$J_\mu^{(l),f}(x) = Q_f \bar{\psi}_f(x)\gamma_\mu\psi_f(x), \tag{2.3}$$
$$J_\mu^{(ps),f}(x) = \frac{Q_f}{2}\left[\bar{\psi}_f(x+\mu)U_\mu^\dagger(x)e^{-iaB_\mu}(\gamma_\mu+1)\psi_f(x) + \bar{\psi}_f(x)U_\mu(x)e^{iaB_\mu}(\gamma_\mu-1)\psi_f(x+\mu)\right].$$

The vacuum polarization tensor thus reads in our setup

$$\Pi_{\mu\nu}^{(ps,l),N_f}(q^2) = \int d^4x e^{iqx}\left\langle J_\mu^{(ps),N_f}(x) J_\nu^{(l),N_f}(0)\right\rangle. \tag{2.4}$$

While the local current is not conserved, it allows us to reduce the number of inversions needed for the determination of the vacuum polarization, with respect to the case where the point-split current would be used at both source and sink.

## 3. The Adler function

To determine the Adler function from eq. (1.1) it is necessary to compute the derivative of the vacuum polarization function. We have developed three different procedures to obtain the derivative in order to check for systematic effects. For the first procedure, we start by fitting a Padé-Ansatz to the vacuum polarization,

$$\Pi_{fit}(q^2) = c_0 + q^2\left(\frac{c_1}{q^2+c_2^2} + \frac{c_3}{q^2+c_4^2}\right). \tag{3.1}$$

For the other procedures, we profit from the fact that the use of twisted boundary conditions yields a sufficient amount of data points to determine the derivative of $\Pi(q^2)$ numerically in small steps of $q^2$. To compute the derivative we use fits at different values of $q^2$ separated by a certain step size $\varepsilon$. At each value of $q^2$ we use several fit intervals $q^2 \pm \varepsilon$, where $\varepsilon \in [0.02, 1.0]\,\mathrm{GeV}^2$. In figure 1 the result for the vacuum polarization on the N6 ensemble is shown. We stress that the fit window used

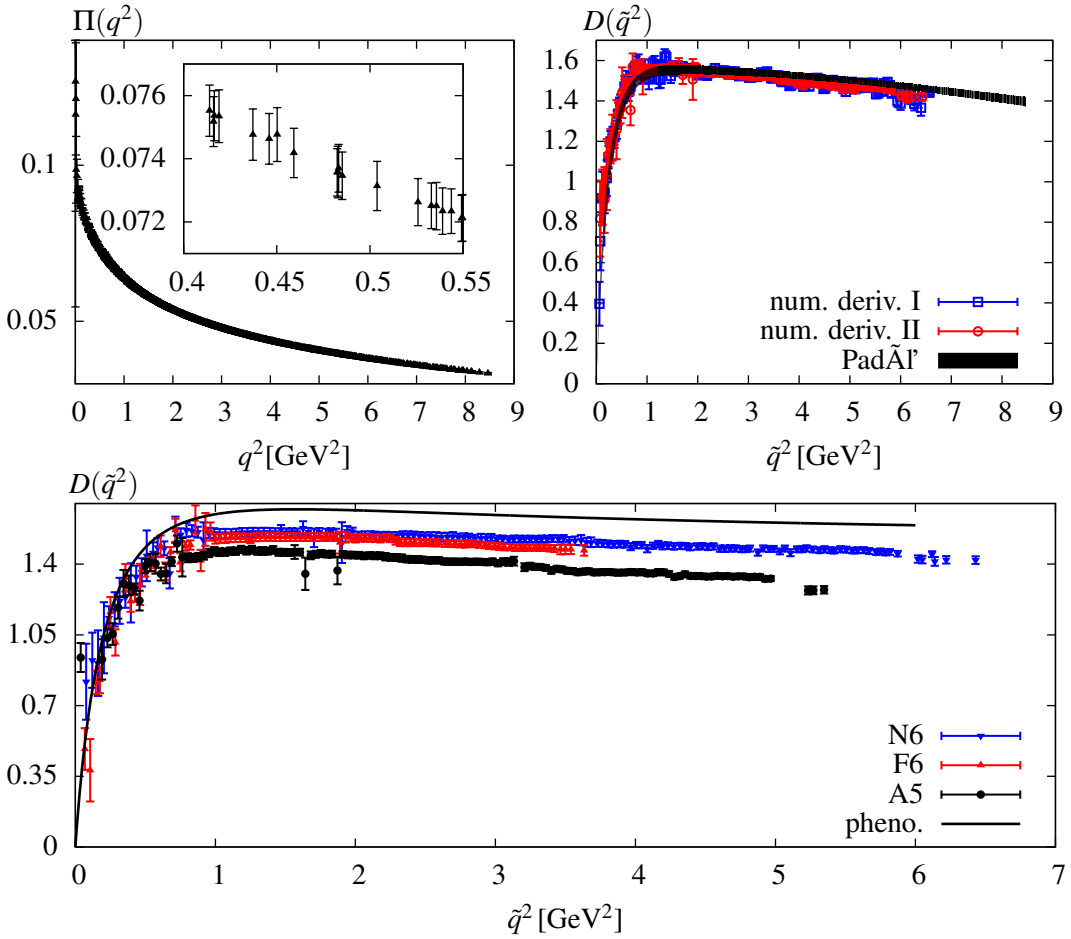


**Figure 1:** Top left: Results for the vacuum polarization on the N6 ensemble. Top right: Comparison of different procedures for the numerical derivative of $\Pi(q^2)$. Bottom: Results for numerical procedure II as an example for the three ensembles N6, F6, and A5 with three different values of the lattice spacing, cf. table 1. To compare the results to a phenomenological model [6] we rescale $q^2 \to \tilde{q}^2 = q^2(m_\rho^{phys}/m_V^{lat})^2$, i. e. the rho mass at the physical point divided by the vector meson mass measured individually on each ensemble.

in the small momentum region should be small enough to describe the curvature of $\Pi(q^2)$, but not too small so as to avoid strong fluctuations due to the limited number of data points. For the large momentum region we find that large fit intervals are more suitable to describe $\Pi(q^2)$, because as $q^2$ is increased fewer points are available for the fit, and the curvature is rather small. We use two different procedures to decide which fit interval describes the numerical derivative best.

The first numerical procedure uses linear fits, $\Pi^{[l]}_{fit}(q^2) = a_l + b_l q^2$. We look for a region in $\varepsilon$ where the coefficient $b_l$ is stable.

The second numerical procedure uses linear, $\Pi^{[l]}_{fit}(x) = a_l + b_l x$, and quadratic fits, $\Pi^{[q]}_{fit}(x) = a_q + b_q x + c_q x^2$, where $x = \ln\left(q^2\right)$. The use of the variable $x$ is motivated by the linear behaviour of $\Pi(x)$ in the interval of $q^2 \in [1,10]\,\mathrm{GeV}^2$, and the second order term is used to choose the appropriate fit window by constraining deviations from the linear behaviour. In the top right panel of figure 1 we compare the different procedures and find an overall good agreement among the methods. The

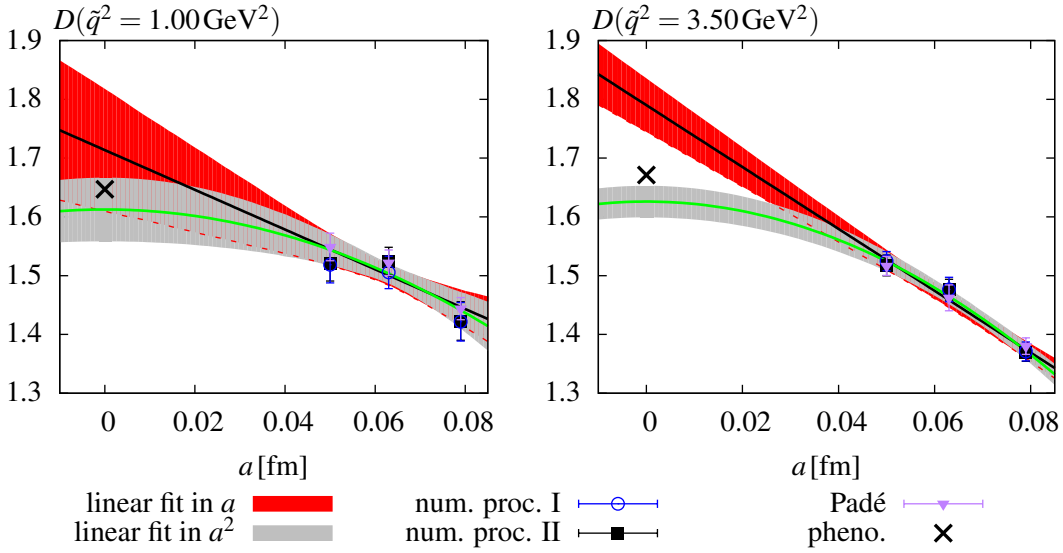


**Figure 2:** Results for extrapolations to the continuum using linear fits in $a$ and in $a^2$ to numerical procedure II at two different momentum transfers. For comparison the values determined by the other procedures for the Adler function are shown as well.

panel on the bottom of figure 1 shows the result for the Adler function for three different lattice spacings. Note that the ensembles considered in figure 1 are not at a fixed pion mass as needed to properly identify the lattice spacing dependence. The comparison to the phenomenological curve should be regarded as qualitative at this stage. In figure 2 the momentum transfer is rescaled by $q^2 \to \tilde{q}^2 = q^2(m_\rho^{phys}/m_V^{lat})^2$ [11] and the continuum extrapolation illustrated at two different momentum transfers, $\tilde{q}^2 = 1.0\,\mathrm{GeV}^2$ and $\tilde{q}^2 = 3.5\,\mathrm{GeV}^2$. As expected the signs of cut-off effects increase with $q^2$. We apply linear fits in $a$ and in $a^2$ to test the continuum limit scaling.

## 4. The Ward identity of the vacuum polarization

The introduction of twisted boundary conditions in the computation of the vacuum polarization tensor requires the use of different twist angles, $\Theta^{(1)} \neq \Theta^{(2)}$, in each of the two quark propagators appearing in $\Pi_{\mu\nu}$. This leads to a breaking of isospin symmetry which introduces modifications to the Ward identities in eq. (1.2). The net effect of the twisted boundary conditions on the Ward identity enters through the background field $B_\mu^{(j)} = \Theta_\mu^{(j)}/L$. It should thus vanish in the infinite volume limit. We perform a dedicated study of the lattice Ward identity in order to monitor the possible impact on our calculation of the vacuum polarization function. To this end we define the quantity

$$W_\nu^{(ps)}(q^2) = \left\langle \left| \sum_\mu q_\mu \Pi_{\mu\nu}^{(ps,l)}(q^2) \right| \right\rangle_{q^2}, \tag{4.1}$$

where the absolute value of the sum is averaged over degenerate values of $q^2$ to avoid compensating effects. The results shown in figure 3 indicate that for vanishing twist angle the Ward identity of the point-split current is fulfilled almost to machine precision. For non-vanishing twist angles we

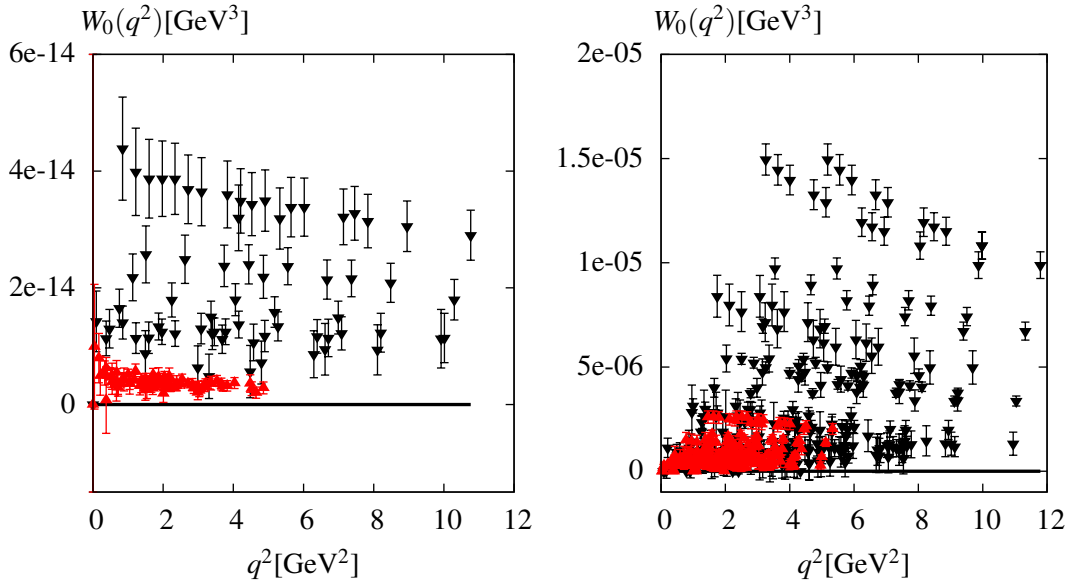


**Figure 3:** The determination of $W_0$ in eq. (4.1) for E5 with L=2.0 fm are shown as red triangles facing up, while the black triangles facing down refer to results on F6 with L=3.0 fm. Left: $W_0(q^2)$ at vanishing twist angle. Right: $W_0(q^2)$ for the largest twist angle of $\Theta = \frac{9\pi}{10}$ that we use in simulations.

observe that the Ward identity in eq. (1.2) is modified. We confirm that this effect diminishes as the volume is increased.

To quantify the possible impact of the violation of the Ward identity in the extraction of the vacuum polarization function $\Pi(q^2)$, we consider the following dimensionless ratios

$$A_\nu^{(ps)}(q^2) = \frac{W_\nu^{(ps)}(q^2)}{q_\nu q^2 \langle \Pi(q^2) \rangle_{q^2}}, \quad B_\nu^{(ps)}(q^2) = \frac{\sum_\mu q_\mu \Pi_{\mu\nu}^{(ps,l)}}{q_\nu \Pi_{\nu\nu}^{(ps,l)}}, \tag{4.2}$$

where the latter is similar to what was used in [12]. Contrary to the case of $A_\nu^{(ps)}(q^2)$, we observe that $B_\nu^{(ps)}(q^2)$ can lead to isolated peaks for some values of $q^2$. This effect appears to be due to rather small values of the denominator of $B_\nu^{(ps)}(q^2)$ in the case of $\nu = 1$ direction, where the twist is applied. We show the results for these ratios in figure 4, and find that for the current precision of our calculations, the violation of the Ward identity induces a negligible effect on the determination of the vacuum polarization function.

## 5. Conclusions and outlook

We presented three different methods to compute the Adler function from vacuum polarization data which agree within errors over a large range of momentum transfer. Furthermore we performed a preliminary study of the continuum limit scaling in the large $q^2$ regime. In the future we plan to extract the hadronic contribution to the running of $\alpha_{\rm QED}$, which requires an extrapolation to the continuum limit and a proper analysis of the $m_\pi$-dependence.

We presented numerical results for the Ward identities at different lattice volumes at a single lattice spacing that signal modifications of the usual Ward identities in the presence of twisted boundary conditions. This effect diminishes as the volume is increased, and given the current precision of

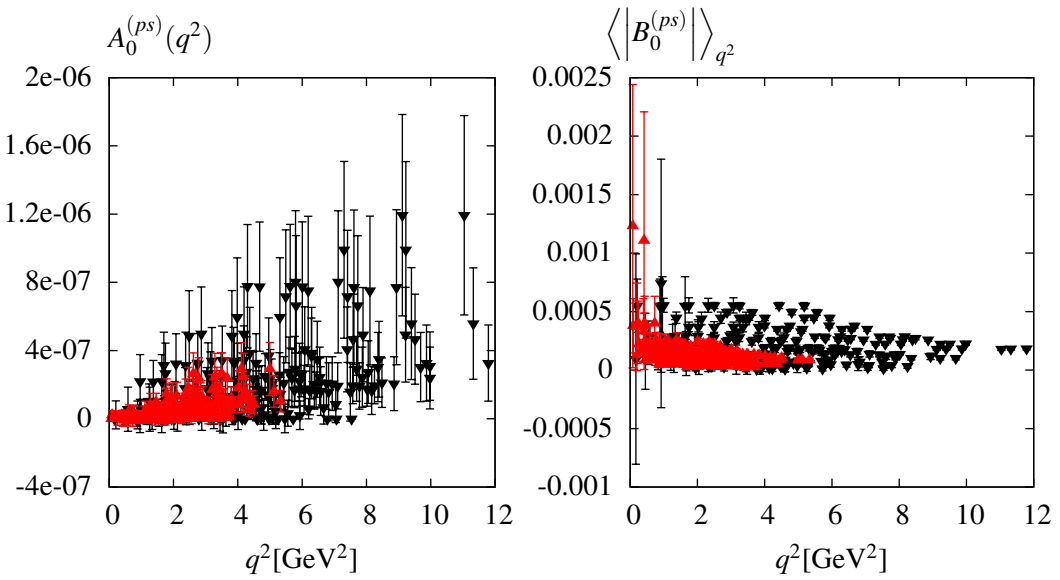


**Figure 4:** Results for $A_V^{(ps)}(q^2)$ and $B_V^{(ps)}(q^2)$ for $\Theta = \frac{9\pi}{10}$ are shown in the plots on the left and right, respectively. Black triangles facing up refer to results for E5, L=2.0 fm, red triangles facing down to results for F6, L=3.0 fm.

our calculations of the vacuum polarization it is observed to be negligible.

Acknowledgements: Our calculations were performed on the "Wilson" HPC Cluster at the Institute for Nuclear Physics, University of Mainz. We thank Dalibor Djukanovic and Christian Seiwerth for technical support. We are grateful for computer time allocated to project HMZ21 on the BlueGene computers "JUGENE" and "JUQUEEN" at NIC, Jülich. This research has been supported in part by the DFG via the SFB 1044.

## References

[1] S. L. Adler, Phys. Rev. D **10** (1974) 3714.

[2] F. Jegerlehner, Nucl. Phys. Proc. Suppl. **181-182** (2008) 135, arXiv:0807.4206.

[3] M. Della Morte, B. Jäger, A. Jüttner and H. Wittig, JHEP **1203** (2012) 055, arXiv:1112.2894.

[4] https://twiki.cern.ch/twiki/bin/view/CLS/WebIntro.

[5] S. Capitani et al, PoS LATTICE **2011** (2011) 145, arXiv:1110.6365.

[6] A. Francis, B. Jäger, H. B. Meyer and H. Wittig, Phys. Rev. D **88** (2013) 054502, arXiv:1306.2532.

[7] M. Della Morte and A. Jüttner, JHEP **1011** (2010) 154, arXiv:1009.3783.

[8] C. T. Sachrajda and G. Villadoro, Phys. Lett. B **609** (2005) 73, hep-lat/0411033.

[9] P. F. Bedaque and J. -W. Chen, Phys. Lett. B **616** (2005) 208, hep-lat/0412023.

[10] G. M. de Divitiis, R. Petronzio and N. Tantalo, Phys. Lett. B **595** (2004) 408, hep-lat/0405002.

[11] X. Feng, K. Jansen, M. Petschlies and D. B. Renner, Phys. Rev. Lett. **107** (2011) 081802, arXiv:1103.4818.

[12] C. Aubin, T. Blum, M. Golterman and S. Peris, Phys. Rev. D **88** (2013) 074505, arXiv:1307.4701.